Fuel 381 (2025) 133448

Contents lists available at ScienceDirect

Fuel

journal homepage: www.elsevier.com/locate/fuel

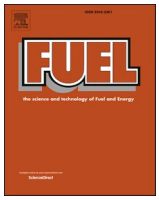

Full Length Article

A study of the mechanisms associated with CO_2 utilisation via the reverse Boudouard reaction

Ahmed Mohammed Alsawadi [a,*], Richard Marsh [a], Julian M. Steer [a], David Morgan [b]

[a] Cardiff School of Engineering, Cardiff University, Queen's Buildings, The Parade, Cardiff CF24 3AA, United Kingdom
[b] Cardiff Catalysis Institute, School of Chemistry, Cardiff University, Park Place, Cardiff CF10 3AT, United Kingdom

ARTICLE INFO

Keywords:
Boudouard reaction
Char reactivity
Demineralisation
Char structure
CO_2 Chemisorption
Kinetic models

ABSTRACT

The main purpose of this work was to investigate the critical mechanisms affecting char reactivity in CO_2 gasification. This research investigated the influence of physical and chemical properties of biochar, hydrochar and coal char samples during CO_2 gasification using a variety of laboratory techniques to measure properties including mineral content, porosity, microcrystalline structure, morphology, surface elements and surface functional groups. These were characterised by inductively coupled plasma (ICP-OES) analysis, nitrogen adsorption analysis, X-ray diffraction (XRD), scanning electron microscopy combined with energy dispersive spectroscopy (SEM-EDS) and X-ray photoelectron spectroscopy (XPS).

Furthermore, this study examined CO_2-chemisorption measurements of the char samples to measure both organic and inorganic active sites using thermogravimetric analysis. The CO_2-chemisorption method at low temperatures was implemented to quantify the amount of CO_2 adsorbed/desorbed within the char's surface and to identify its role in char reactivity.

Key findings include that while the pore structure of chars is indeed a significant characteristic, porosity alone does not exert the primary influence on gasification reactivity. Gasification reactivity was well correlated with CO_2 strong chemisorption capacities and kinetic models, which were used to describe CO_2 gasification by fitting experimental data with these models.

1. Introduction

The recent interest in Carbon Capture, Utilisation and Storage (CCUS) can be attributed to its potential as a solution to the emission of CO_2 via a circular economy approach where CO_2 can be effectively recycled within the industrial environment, especially where sustainable biomass is integrated into the system [1]. Carbon capture and utilisation (CCU) is considered a potential net zero technology and an alternative to Carbon Capture and Storage (CCS) [2]. According to the International Energy Agency (IEA) [3], the utilisation of CO_2 consists of two pathways, which are non-conversion and conversion methods. In the non-conversion approach, CO_2 can be directly used without undergoing chemical changes. The conversion approach involves utilising CO_2 as a feedstock, which is then chemically converted to value-added products.

Different technologies for CO_2 conversion to fuels and chemical products have been explored by research groups. Thermochemical, electrochemical, biological and catalytic conversion methods have been reported in the literature [4–6,7–9]. All of these efforts are focused primarily on mitigating the CO_2 footprint although each method has its own limitations and strengths over the other approaches, such as production yield, energy requirement [8,10]. In this context, one potential conversion technology route is the use of biomass gasification as a thermochemical means to convert renewable sources of carbon into valuable chemical products, e.g. reduction to CO as a primary chemical for subsequent downstream deployment for organic chemical feedstocks [11]. In such a gasification process, CO_2 mitigation can be achieved through the reverse Boudouard reaction Eq. (1) by directly using CO_2 as a gasifying agent with bio-derived carbon-based material to form CO. This simple reaction produces highly pure CO, which reduces the overall process cost [12].

$$C + CO_2 \rightleftharpoons 2CO \quad (1)$$

The reverse Boudouard reaction is an endothermic heterogeneous reaction that requires a high temperature, typically >700 °C to shift the

* Corresponding author.
E-mail address: alsawadiam@cardiff.ac.uk (A.M. Alsawadi).

https://doi.org/10.1016/j.fuel.2024.133448
Received 29 February 2024; Received in revised form 30 September 2024; Accepted 14 October 2024
Available online 29 October 2024

Table 1
Proximate and ultimate analysis of char samples.

Sample	Proximate analysis (wt.%, d)			Ultimate analysis (wt.%, d, daf)				
	V	A	FC[a]	C	H	O[a]	N	S
BC1	17.6	4.7	77.7	81.7	2.3	14.1	1.9	0.02
BC2	12.6	2.6	84.8	85.2	2.6	10.9	1.3	0.03
BC3	4.5	37.0	58.5	55.9	0.5	41.5	1.5	0.54
BC4	10.0	21.0	69.0	68.5	0.9	28.4	2.0	0.17
CC	18.3	17.6	64.1	76.0	2.6	18.2	3.0	0.26
HC	56.7	21.2	22.1	47.7	4.8	45.4	1.7	0.45
BC1HCl	17.1	2.8	80.1	84.1	2.2	13.8	0.01	–
HCHCl	66.0	3.5	30.5	56.3	5.4	35.2	2.6	0.6

FC, fixed carbon; V, volatile matter; A, ash content; d, dry basis; daf, dry ash free basis;
[a] by difference.

chemical equilibrium towards CO production [13]. Therefore, understanding the mechanism of the Boudouard reaction with inhomogeneous materials such as biochars and studying the factors that affect the reaction rate is beneficial to increase the gasification process effectiveness and hence reduce technology risks in process up-scaling. This study therefore aims to investigate both physical and chemical features of various carbonaceous materials and the correlation of these properties with CO_2 Boudouard gasification reactivity. Three kinetic models were employed in this paper to measure kinetic parameters, namely, the Volumetric Model (VM), Grain Model (GM) and Random Pore Model (RPM). These models were selected because of their different behaviour relating the reaction mechanism between CO_2 and char particles.

2. Materials and methods

2.1. Sample preparation

In this study, a range of commercially supplied carbonaceous materials with different properties were chosen for the experiments, these include biochars, coal char and hydrothermally carbonised char (hydrochar). Four were biomass chars, two from recovered wood and two from wastewater sludge, both biochar types were produced through pyrolysis. Because these were commercially supplied samples the specific pyrolysis conditions were subject to confidentiality. The coal char was made using a drop tube furnace (DTF) at 1100 °C at a residence time of 35 ms, as detailed in previous work by the authors [14]. Hydrochar was produced from high plastic content anaerobic digestion (AD) fibre in a hydrothermal carbonisation plant [15]. In the hydrothermal carbonisation process (HTC), the solid residue from digested food waste was subjected to high temperature in an aqueous environment at 200 °C to produce the hydrochar. The char samples were labelled as BC1 and BC2 for wood chars; BC3 and BC4 for sewage sludge chars; CC for coal char and HC for hydrochar.

A demineralisation process with hydrochloric acid (5 wt% HCl) solution was carried out following a washing method from literature [16]. Dried and sieved samples of both BC1 and HC were chosen for demineralisation treatment due to their higher reactivity compared to the other chars in this work. In this process, 12.5 g each of BC1 and HC were added to 125 ml of the prepared washing solutions in flasks, shaken manually, and left for 24 h at room temperature to dissolve completely. The mixtures were then washed with deionised water and subjected to vacuum filtration to separate the solid char particles from the solutions. Finally, the washed samples were dried in an oven at 105 °C for an additional 24 h, and were denoted BC1HCl and HCHCl.

2.2. Pretreatment and initial characterisation

Prior to the experiments, the samples were dried at 105 °C for two hours until a constant weight was achieved following the standard BS EN ISO 18134–3:2015. All samples were then ground by a ring mill and subsequently sieved using the standard BS ISO 1953:2015 to reduce particle size to 100 % less than 250 μm. The volatile matter content was determined based on the standard methods BS EN ISO 18123:2015. Measurement of the ash content for both biomass char and coal char were carried out according to the standard BS EN ISO 18122:2015 and BS ISO 1171:2010, respectively. The proximate and ultimate analyses results are listed in Table 1 and were repeated in quadruplicate and duplicate, respectively.

The organic elements (carbon, hydrogen, nitrogen, sulphur) were determined using a Thermoscientific-FlashSmart™ Elemental Analyser and LECO carbon and sulphur analyser LECO-SC-144DR. For Inductively Coupled Plasma Optical Emission Spectroscopy (ICP-OES), a PerkinElmer Avio® 220 Max was used to analyse the chemical compositions of the ash. Mineral phase identification and semi-quantification was carried out using an X-ray diffraction (XRD) Siemens-Diffractometer/D5000. The diffraction was collected from 10° to 80° 2 theta at a scan speed of 0.02 degrees per second using copper radiation at 35 kV and 40 mA. Nitrogen adsorption analysis was conducted at −196 °C in a Quantachrome QuadraSorb SI surface area and pore size analyser to measure surface areas, micropore volume, total pore volume and pore size of the tested chars. Prior to the measurements, 0.2 g of dried char samples were degassed in a vacuum at 250 °C for < 24 h. The Brunauer-Emmett-Teller (BET), t-plot and the Barret-Joyner-Halenda (BJH) desorption methods were used to determine specific surface area, S_{BET}; micropore surface area and micropore volume, S_{Micro} and V_{Micro}; and average pore size diameter, D_p. The total pore volume, $V_{Total,}$ was calculated based on the amount of N_2 adsorbed at a relative pressure of $P/P_0 = 0.938–0.956$. The morphology and distribution of elements on the surfaces of the chars were observed by scanning electron microscopy coupled with energy dispersive spectroscopy (SEM-EDS), which included SEM: Zeiss Sigma HD field emission gun SEM, 20 kV beam energy, ~1.5nA beam current using a 60 μ m diameter final aperture. For chemical analysis, samples were mounted on aluminium SEM stubs using carbon adhesive tabs, coated with a 15 nm thick layer of carbon prior to being loaded in the SEM. Two 150 mm^2 Oxford Instruments X-Max silicon drift detectors were used for semi-quantitative Energy Dispersive Spectroscopy (EDS) analysis. Backscattered electron images and EDS spectra were acquired and processed using Oxford Instruments Aztec software. EDS results were quantified using factory standards and data was normalised to 100 %.

X-ray photoelectron spectroscopy (XPS) was performed on a Kratos Axis Ultra DLD system using a monochromatic Al *Kα* X- source operating at 144 W (12 mA × 12 kV). Data was collected with pass energies of 160 eV for survey spectra, and 40 eV for the high-resolution scans with step sizes of 1 eV and 0.1 eV respectively. The system was operated in the Hybrid mode, which uses a combination of magnetic immersion and electrostatic lenses for high sensitivity and acquired using the slot aperture which gives an analysis area of *ca.* 300 × 700 μm^2. As samples were electronically isolated form the spectrometer, a magnetically confined charge compensation system was used to minimise charging of the sample surface, and all spectra were taken with a 90° take-off angle. A base pressure of ca. 5×10^{-9} Torr was maintained during collection of the spectra. Data was analysed using CasaXPS (v2.3.26) [17], after calibration to the lowest energy C 1s peak taken to be 284.5 eV. Analysis was performed using a Shirley background to account for electron scattering and using modified Wagner sensitivity factors as supplied by the manufacturer.

2.3. Isothermal CO_2 gasification tests

One of the most commonly used methods to investigate the isothermal CO_2 gasification and kinetics of chars is thermogravimetric analysis (TGA). In this study, gasification experiments were carried out in the Mettler-Toledo TGA/DSC 3^+ STAR®, analysing 15 mg of the char sample in an alumina crucible. The isothermal gasification experiments were conducted at three selected temperatures 900 °C, 950 °C and 1000

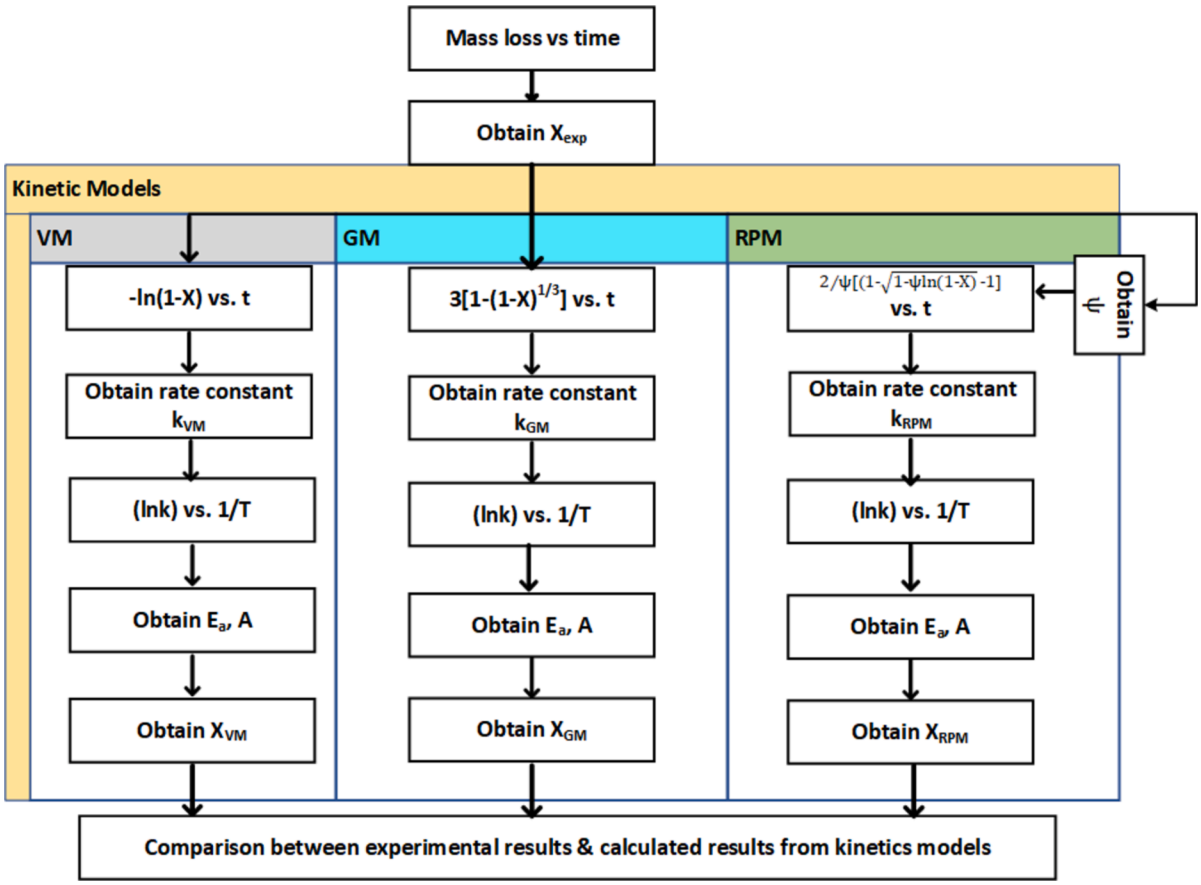

Fig. 1. Flowchart procedures to determine the kinetic model parameters.

°C. In each run, the sample was heated to 900 °C in 100 ml/ min of N_2 flow at a heating rate of 20 °C /min and held at that temperature for 7 min to remove the volatile matter before switching to the CO_2 flow. This holding period and temperature was chosen based on the standard volatile matter content method to generate a 'fixed carbon' produced in repeatable conditions as a consistent baseline for CO_2 gasification comparisons. The sample was then heated to the target gasification temperature and N_2 was replaced by CO_2 with a flow rate of 100 ml/ min. The final temperature was held constant until the conversion was completed. This work presents a comparison of the gasification reaction, via the reverse Boudouard reaction, of the 'fixed carbon' portion of the different samples. In the current work, the pyrolysis data have been excluded from TGA results, and just the CO_2 gasification stage is presented. A typical TGA curve of the complete experimental method is provided in the supplementary material (Fig.S1), showing pyrolysis and reverse Boudourd gasification phases as well as initial mass considered for the calculation of CO_2 reactivity. Each test was performed at least twice to ensure reliability, and relative standard error was less than 5 %.

The experimental conversion (X_{exp}) of the gasification was obtained using following equation:

$$X_{exp} = \frac{m_i - m_t}{m_i - m_f} \tag{2}$$

where m_i represents the post pyrolysis mass after N_2 switched to CO_2, m_t is the measured mass at time t and m_f is the final mass remaining after complete gasification. Gasification reactivity at different temperatures was evaluated using the reactivity index $R_{0.5}$ (s^{-1}) as proposed by Takayuki et al. [18], expressed by the following equation:

$$R_{0.5} = \frac{0.5}{t_{0.5}} \tag{3}$$

where $t_{0.5}$ denotes the time in seconds required to convert 50 % of the sample. Consequently, chars with a shorter $t_{0.5}$ gasification time are more reactive than those with longer $t_{0.5}$ gasification times [19].

2.4. Kinetic models

The gasification reaction rate of char is often used to describe the universal gasification reaction of carbonaceous material as a function of conversion, temperature and pressure using the following equation [20]:

$$\frac{dX}{dt} = k(T, P_{CO_2}) f(X) \tag{4}$$

where k is the apparent gasification reaction rate constant, which is dependent on the reaction temperature (T) and CO_2 partial pressure (P_{CO_2}), and $f(X)$ is a conversion function that indicates the reaction model being employed for the gasification process. The Arrhenius equation can be used to define the reaction rate constant k under the assumption that the partial pressure of CO_2 remains constant while the reaction proceeds and is only influenced by temperature, which is given by:

$$k = A_0 e^{-E/RT} \tag{5}$$

where A_0, E and R are the pre-exponential factor, activation energy and universal gas constant, respectively.

2.5. Volumetric model

The volumetric model (VM) [21], also referred to as the homogeneous model is based on the assumption that the interaction between the solid particle and the reactant gas occurs uniformly throughout all active

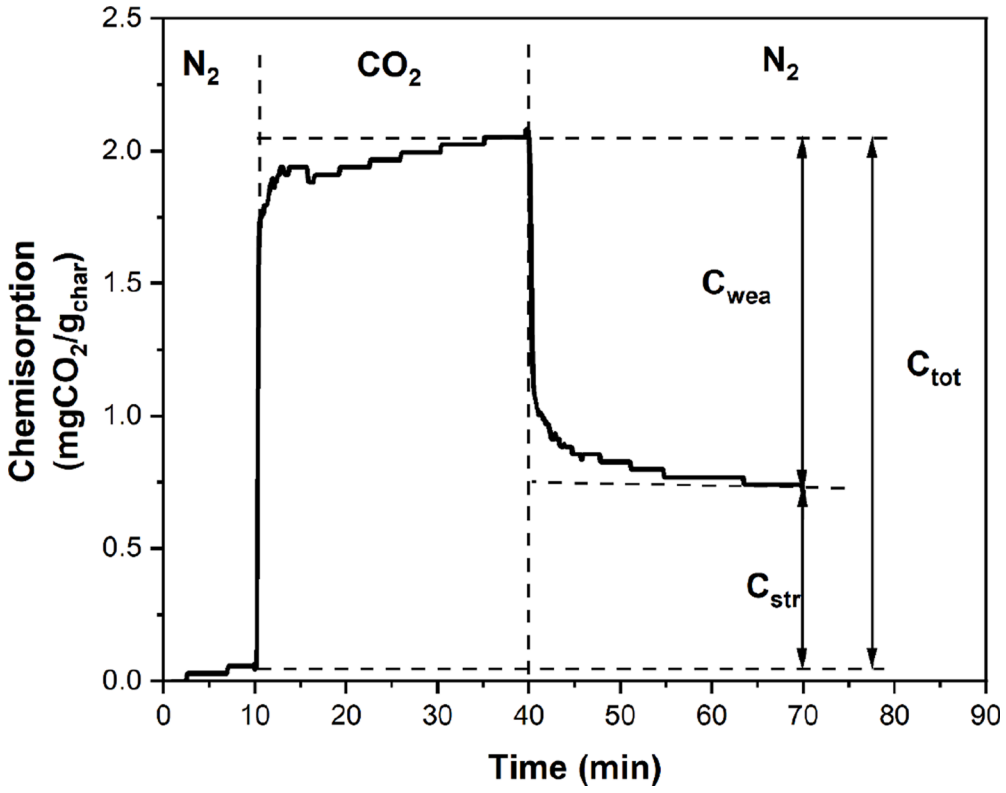

Fig. 2. Example of CO_2 chemisorption of BC4.

sites within the char particle, whether located externally or internally [22]. Consequently, the reaction rate is proposed to decrease linearly with carbon conversion [23]. This model takes into account that although particle density fluctuates during char gasification, particle size remains constant [24]. The reaction rate equation of the VM is written as:

$$\frac{dX}{dt} = k_{VM}(1 - X) \tag{6}$$

2.6. Grain model

The grain model or the shrinking core model was proposed by Sezekely and Evans [25]. According to the GM, char structure consists of numerous numbers of spherical or cylindrical particles and the reaction takes place at the outer surface of these particles. As the reaction progresses, the char particles shrink in size and only the ash layer remains. Assuming that the particles have a spherical shape, the GM is expressed by the following equation:

$$\frac{dX}{dt} = k_{GM}(1 - X)^{2/3} \tag{7}$$

2.7. Random pore model

The main consideration of the random pore model is the overlapping of pore structure, which reduces the available surface area for the reaction [26,27]. The overall reaction rate is expressed as:

$$\frac{dX}{dt} = k_{RPM}(1 - X)\sqrt{1 - \psi ln(1 - X)} \tag{8}$$

The experimental conversion results were compared with that predicted from the kinetic models. The following equation was used to calculate the deviation $DEF(X)(\%)$ between the experimental and predicted data [28]:

$$DEF(X)(\%) = 100 \times \frac{\sqrt{(\sum_{i=1}^{N}(X_{exp,i} - X_{model,i})^2/N)}}{\max(X)exp} \tag{9}$$

where $DEF(X)(\%)$ is relative error, $X_{exp,i}$ is experimental conversion data, $X_{model,i}$ is the conversion degree value calculated by the three models, $\max(X)exp$ is the maximum conversion of the experiment and N is the total number of data. Fig. 1 illustrates the calculation procedure that was used to find kinetic parameters obtained by the VM, GM and RPM models.

2.8. CO_2 chemisorption

Chemical adsorption of CO_2 is used to measure the availability of active sites for CO_2 to combine with the surface of a material. The combination of gas phase CO_2 with the solid sample is essential to the char gasification reactivity [29]. In this work, measurement of CO_2 chemisorption was conducted in the TGA apparatus by following the method described in the literature [29,30]. In each chemisorption test, a platinum crucible was filled with about 40–50 mg of char. Under a N_2 atmosphere, the sample was heated to 850 °C with a heating rate of 30 °C/min, and the temperature was held for 30 min to prepare the char surface for the adsorption process. The char sample was subsequently cooled to 300 °C at 10 °C /min. At that temperature, the sample was held for an additional 30 min, and the temperature remained constant until the end of the test. N_2 was then replaced with CO_2, the CO_2 chemisorption proceeded, and the change in the sample weight as a function of time was recorded. In order to eliminate any remaining weakly chemisorbed CO_2 molecules, the gas was switched back to N_2 after 30 min of adsorption, and the sample was degassed for another 30 min. Throughout the experiment, a constant flow rate of 100 mL/min was employed for the flow of both N_2 and CO_2. The chemisorption experiment was blank corrected by subtracting a blank curve recorded of an

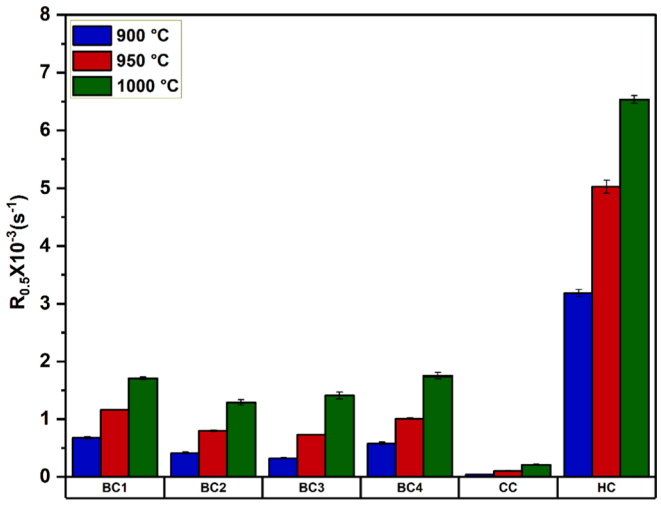

Fig. 3. CO_2 gasification reactivities of chars at different temperatures.

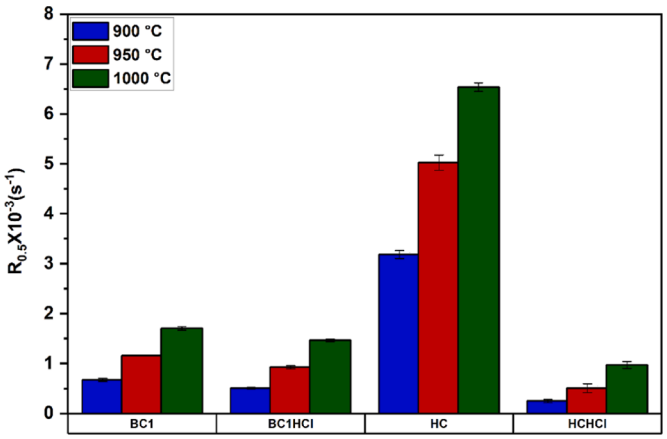

Fig. 4. Comparison of raw biochar and hydrochar reactivities before and after acid treatment.

empty crucible. The relative standard deviation for each test performed in this research was less than 3 % over three independent runs, indicating good repeatability. Fig. 2 shows an example of CO_2 chemisorption for BC4.

3. Results and discussion

3.1. Gasification reactivities

For this approach to be considered as a means to produce carbon monoxide as a chemical intermediate to utilise carbon dioxide, the char reaction needs to take place at the lowest temperature and for the shortest time, to minimise the overall energy input for the reaction.

The six chars' reactivities were measured at three different temperatures to compare the effect of this parameter on the reactivity at 900 °C, 950 °C and 1000 °C shown in Fig. 3. It is clear that all the biomass chars are significantly more reactive than the coal char sample at all gasification temperatures, particularly at the lowest temperature.

The hydrochar (HC) reactivity was superior to the others, with reactivity values of 3.19×10^{-3}, 5.03×10^{-3} and 6.54×10^{-3} s^{-1} at temperatures of 900 °C, 950 °C and 1000 °C, respectively. The reactivity values of HC are around 4 times higher than the most reactive biochar in this study, namely, BC1. Research carried out by Lanhijani and coworkers [31] also found that hydrothermal carbonisation (HTC) treatment of biomass enhanced the CO_2 gasification reactivity of the char produced. In comparison to the hydrochar, the results in Fig. 3, show a narrower difference in the reactivities of the other samples derived from woody biomass and pyrolysed sewage sludge.

To measure the effect of varying masses of 'fixed carbon' remaining after the N_2 pyrolysis; TGA curves were run using different total sample masses (m_{total}) to determine the role of the varying 'fixed carbon' mass left post pyrolysis on the final reactivity. The influence of variations in the fixed carbon on chars' reactivity was examined using a smaller sample size. In this test, 5 mg of the fixed carbon was tested using the same TGA gasification conditions. The results in Fig. S2 show consistent reactivity trends, suggesting that the relative reactivities were a reflection of the intrinsic properties of the char samples and were not significantly affected by the fixed carbon mass.

The results indicate that the gasification reactivity is significantly influenced by the reaction temperature and as expected the reactivity of all the chars exhibit an upward trend as the temperature is elevated from 900 °C to 1000 °C.

The catalytic effect associated with the components contained in the ash has been widely researched. In the context of this approach, the catalytic effect of the mineral components on CO_2 gasification reactivity has been compared between the most reactive chars by acid leaching using hydrochloric acid. The effect of removing minerals from the two chars, BC1 and HC, is shown in Fig. 4; in both cases the reactivities were reduced.

The reactivity of BC1 was reduced by up to 27 %, while the reactivity of HC was reduced by up to 92 %. The large reactivity reduction for the hydrochar demonstrates the importance of the role of the ash components in determining its reactivity. In comparison, the mechanism by which the ash is working in BC1 does not dominate the reactivity to the same extent as HC. Further, the effectiveness of acid wash on the char samples was examined using a paired difference *t*-test to evaluate if a significant difference occurred between the reactivity of non-demineralised samples and reactivity of demineralised sample. The results confirmed that the reduction significantly occurred with p-value of <0.05 for all gasification temperatures range (as shown in Table S1).

The TGA conversion profiles and DTG rate of change profiles illustrate the stark difference of the gasification reactivity of BC1 and HC before and after the washing process, as shown in Fig. 5. The biochar sample, BC1 (Fig. 5(a)), achieved complete conversion between 10 and 25 min depending on the temperature, whereas it took between 13 and 36 min for the demineralised sample, Fig. 5(b), to complete the reaction.

As shown in Fig. 5(c, d), the impact of acid washing on the hydrochar was stronger than biochar. The DTG curve of HC shows maximum weight losses of 16 to 27.5 %/min for the unwashed, but only 0.9 to 4.5 %/min for the washed sample. Although raw char from HC was more reactive than BC1, the demineralised sample of the latter sample showed better reactivity than HCHCl. This suggests that the dominant factor of HC reactivity is the presence of the minerals and their catalytic affect. However, when considering the selection of chars for the CO_2 utilisation reaction using the reverse Boudouard reaction, even after acid washing the two biobased chars were much more reactive than coal char.

3.2. Influence of physical and chemical properties on char reactivity

In the context of the CO_2 gasification reactivity, many researchers have studied factors related to physical structure and chemical properties of char and operational conditions. Specifically, porosity and surface area; the catalytic effect of alkali and alkaline earth metals and transition metals; and the availability of active sites. The variability in CO_2 gasification reactivity of carbonaceous materials was the focus in these studies to determine the likely strongest factors.

3.2.1. Porosity and surface area

In this work, N_2 adsorption at −196 °C was employed to investigate the physical properties of the char samples, owing to its affordability and availability. However, it should be noted that, access of the smallest

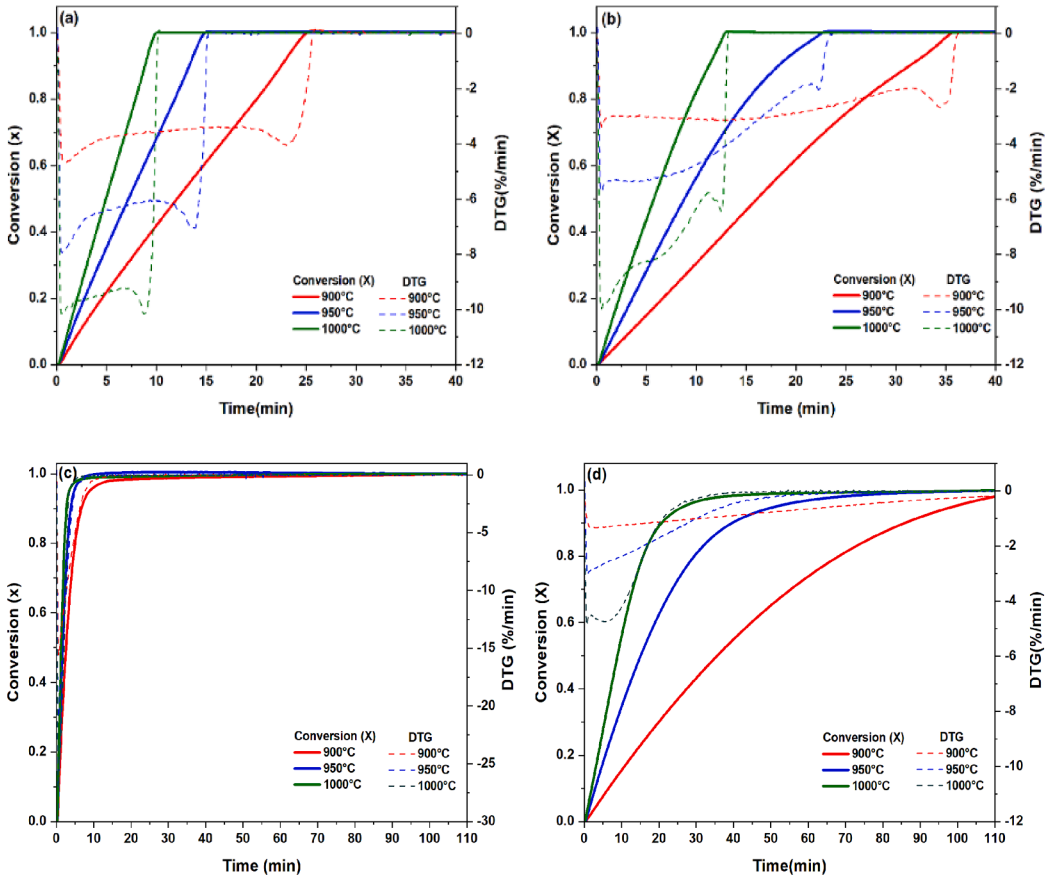

Fig. 5. Carbon conversion profiles and DTG curves of the isothermal gasification step for raw chars and their demineralised chars: (a) BC1, (b)BC1HCl; (c) HC, (d) HCHCl.

Table 2
N_2 adsorption isotherm parameters.

Sample	S_{BET} (m^2/g)	S_{Micro} (m^2/g)	S_{Micro}/S_{BET} (%)	V_{Micro} (m^3/g)	V_{Total} (cm^3/g)	Avg. pore, D_p (nm)
BC1	211.50	53.41	25.25	0.024	0.14	2.58
BC2	261.74	120.76	46.14	0.04	0.16	2.47
BC3	185.53	63.23	34.08	0.03	0.19	4.06
BC4	319.98	173.62	54.26	0.08	0.23	2.88
CC	51.24	15.66	30.56	0.01	0.04	3.04
HC	22.27	–	–	–	0.04	6.87

micropores is limited due to the diffusional limitation of this probe. Alternatively, applying CO_2 at 0 °C for analysis of the ultra-micropores can be effective, particularly for porous solids without polar surface groups, as suggested by IUPAC [32].

There are different theoretical physical adsorption isotherm models which can be used to interpret the experimental adsorption data such as Langmuir, BET, DFT, DR, etc. However, these models cannot provide an absolute value for the specific surface area [33]. According to Al-Ghout et al. [34], choosing the optimum physisorption isotherm model relies on three key criteria, which are the fitting of the experimental data, the thermodynamics of the model function, and the model utility. Recently published study [35], compared the use of N_2 and CO_2 adsorption using BET; the specific surface area results of N_2 and CO_2 physisorption were 676 and 593 m^2/g, respectively. This demonstrates that while N_2 may underestimate very narrow pores, the overall impact on surface area determination is minimal, especially for larger pores, and when using it for just comparison purpose. The relationship between porosity and reactivity for gas–solid reactions where surface area and mass transfer

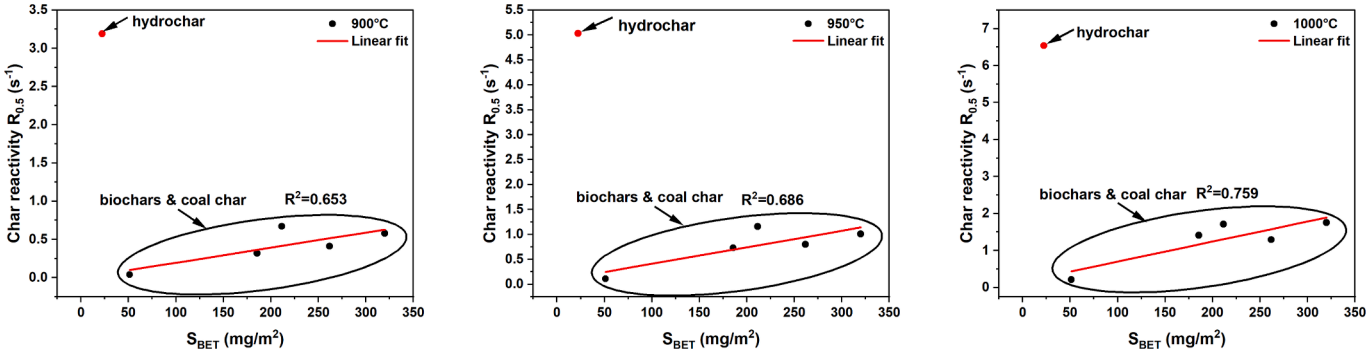

Fig. 6. Correlation between S_{BET} and gasification reactivity.

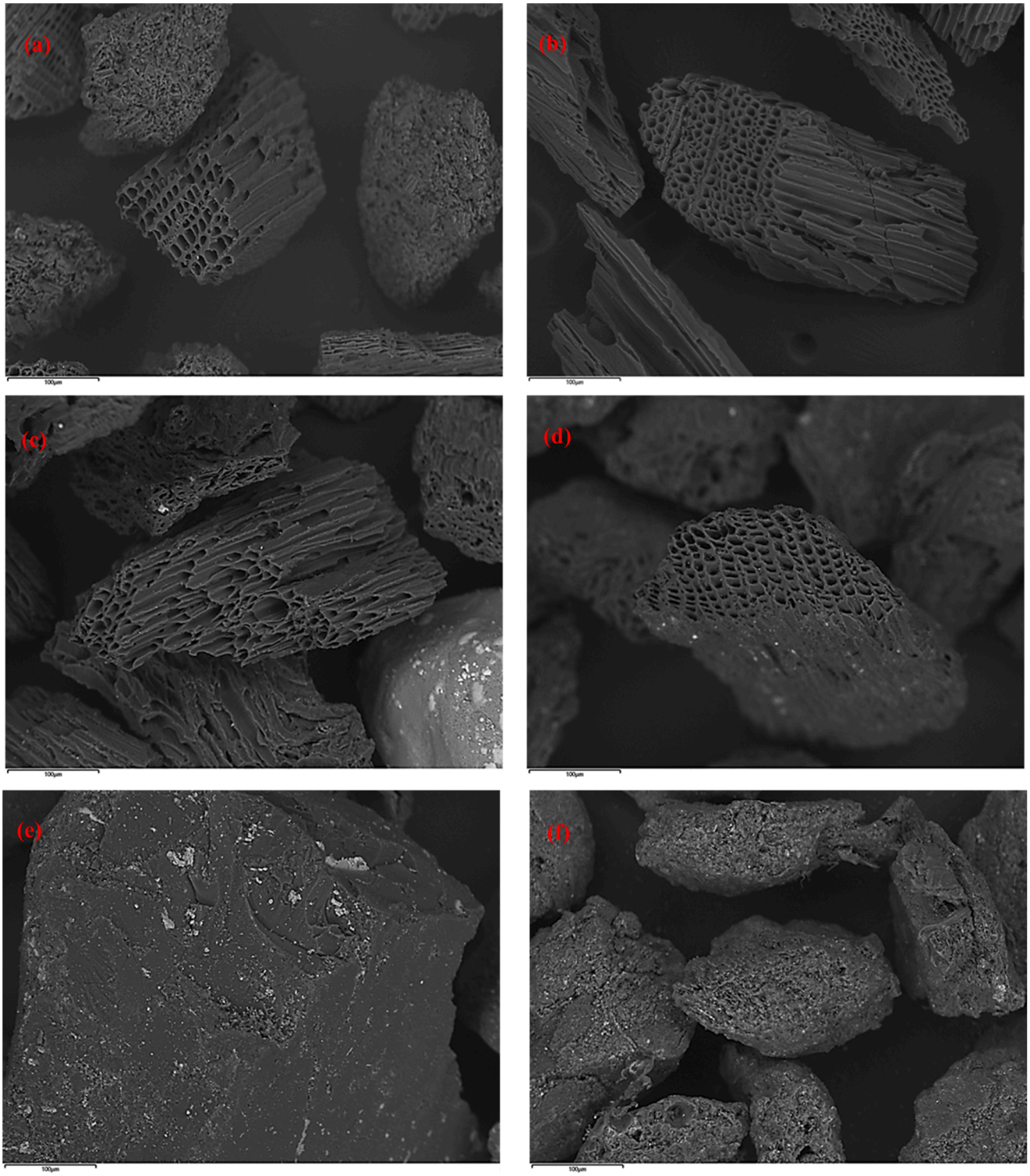

Fig. 7. SEM morphology images of char samples taken at 150X magnification: (a)BC1, (b) BC2, (C) BC3, (d) BC4, (e) CC and (f) HC.

play such a well-documented role has been widely researched. However, the reactivity of hydrochar was not explained by BET surface area as it had the lowest for all chars, with an S_{BET} of 22.27 m^2/g.

For the surface area and isotherm parameters of the chars shown in Table 2, the biomass char samples displayed a variation in structural features. Biomass-derived chars BC1-BC4 had the highest BET, micropore surface areas, and pore volumes compared to hydrochar and the coal char, which showed significantly lower porosity characteristics.

The physical structure differences measured using BET can also be seen in the SEM images in Fig. 7(a, b, c, d). All biomass chars BC1-BC4 exhibit the cellular structure characteristic of bioderived materials, whereas both the hydrochar and the coal char exhibit closed structures Fig. 7(e, f) which is also consistent with the higher pore diameter of 6.87 nm. Coal char has a solid smoothed surface with some cracks and less pores.

Fig. 6 shows the relationship between BET surface areas and chars reactivities at different gasification temperatures. The figure highlights a linear relationship between surface area and reactivity for the set of

Table 3
ICP ash composition analysis of char samples (wt.%, dry basis).

Sample	Fe_2O_3	CaO	MnO	ZnO	Al_2O_3	NiO	K_2O	MgO	Na_2O	P_2O_5	SiO_2	AI
BC1	38.84	35.55	2.52	0.13	1.36	0.01	9.84	5.30	0.97	2.48	3.00	62.17
BC2	15.01	47.13	2.05	0.33	0.72	0.01	19.84	7.27	0.19	4.55	2.90	28.45
BC3	22.57	28.64	0.72	0.47	12.45	0.03	3.53	4.91	1.70	22.85	2.14	60.64
BC4	8.02	51.16	0.75	2.21	15.16	0.04	5.40	6.08	6.43	2.64	2.11	81.30
CC	16.76	10.96	0.19	0.07	53.82	0.04	5.89	3.66	0.89	1.09	6.63	10.91
HC	10.75	55.93	0.24	0.18	8.02	0.01	1.02	3.66	0.55	18.21	1.43	55.14
BC1HCl	44.52	31.61	3.10	0.16	1.99	0.02	3.35	7.70	0.40	3.38	3.77	26.83
HCHCl	34.61	5.20	0.12	0.24	23.25	0.15	2.35	3.55	0.44	7.31	22.78	3.03

chars BC1-BC4, and the coal char. However, the very high reactivity of the hydrochar, combined with the importance of the mineral ash components, flag it as an outlier. It shows no correlation with its porosity. In comparison, these results suggest that porosity is an important factor to describe biochar and coal char reactivity.

3.2.2. Ash mineral content and composition

It is well understood that the presence of metal compounds in the ash can have a catalytic effect on the sample reactivity by promoting electron transfer which facilitates the surface combination of CO_2 with the carbon contained in the sample. The sample demineralisations shown in Fig. 4 for BC1 and HC, demonstrate the particular importance of the ash to the reactivity of the hydrochar after the demineralisation.

However, the results indicate that for the CO_2 gasification reaction the importance of the ash content and composition varies depending on the sample. The biochar samples BC1-BC4 vary in ash between 2.6–37.0 % but the reactivities do not show an equivalent variation. The coal char sample CC contains 17.6 % ash but is much less reactive than BC1 or BC2, which have ash contents of 4.7 and 2.6 % accordingly. The hydrochar sample HC has an ash content of 21.2 % but has much higher reactivity than any of the chars, including BC3 with 37.0 % ash. However, when demineralised its reactivity falls accordingly.

A closer examination of the compositions shows a wide variation in components which is difficult to assign trends to, see normalised figures in Table 3. Calcium's catalytic effect on gasification has been well documented and is present at high levels in the hydrochar, BC3 and BC4. However, BC1 and BC2 have a much lower calcium content (35.55 & 47.13 %) but are much more reactive than the coal char sample CC which has 10.96 % calcium.

What is clear about the coal is the presence of acidic oxides in its ash, based on aluminium and silicon and consequently the base/acid ratio is very low for the coal compared to the other chars. The ratio between the CaO and the sum of Al_2O_3 and SiO_2 is 0.18 for coal compared with 5.93 for the hydrochar. The basicity could play a role in charge transfer which would have an effect on the mechanism of surface interactions. In comparison, a more acidic environment could influence a counter-acting mechanism. The catalytic and inhibition effect of the ash minerals on gasification performance was evaluated through the well-known alkali index. This tool is a simple measurement of the ratio of the basic oxides and the acidic oxides, it is expressed as follows [36]:

$$AlkaliIndex(AI) = \text{Ash}\% \times \left(\frac{Fe_2O_3 + CaO + K_2O + MgO + Na_2O}{Al_2O_3 + P_2O_5 + SiO_2}\right) \quad (10)$$

Alkali index values for the char samples are shown in Table 3. The results revealed that BC1 and HC samples have a high alkali index (62.17 & 55.14 %) and the highest reactivities. However, the alkali index values of sewage sludge derived chars BC3 and BC4 are higher than HC but their reactivity is much lower suggesting other properties are playing a role.

The acid demineralisation treatment shows a corresponding reduction of the AI values by more than 50 % for BC1HCl and HCHCl identifying the importance of ash components on the reactivity. However, even though the AI value for HCHCl was reduced from 55.1 to 3.03, the reactivity is still higher than the coal (CC) with an AI value of 10.9. In this study, it appears that the alkali index alone will not explain the differences in the reactivity.

To further investigate elemental composition and the distribution on the chars' surfaces, five areas were chosen on each char surface to establish the distributions of the elements present on the surface, see Fig. 8. The heavier metal elements back scatter electrons which show-up as light areas distributed through the sample against the darker background of carbon.

Particles of the biochar samples BC1- BC4 exhibit visible open pores corresponding to a cellular structure. The distribution of the ash shows some variation between samples, where BC1, 2 & 3 indicate more isolated distribution where the ash seems to be localised rather than evenly distributed. In comparison, the hydrochar's finely speckled surface suggests a wider distribution on the surface, but it is not strongly visible considering it has a 21.2 % ash content which would suggest it is distributed through the sample rather than on the surface.

The X-ray diffraction patterns of BC1 and the hydrochar HC, before and after acid washing, are shown in Fig. 9 with quantification in Table 4. More crystalline phases of biochar BC1 are visible after acid washing and the BC1HCl diffractogram patterns are more detailed. This phenomenon is due to leaching of the of carbonate minerals that are often effectively dissolved in hydrochloric acid HCl [37], leading to appearance of hidden minerals [38].

The main crystalline components identified in the XRD for the hydrochar (HC) sample are dominated by calcite ($CaCO_3$), with smaller quantities of kaolinite ($Al_2Si_2O_5(OH)_4$), illite ($(K, H_3O)Al_2Si_3AlO_{10}(OH)_2$) and quartz ($SiO_2$). However, after the demineralisation, the hydrochar (HCHCl) is dominated by quartz and an associated significant reduction in reactivity. In comparison, after demineralisation of the BC1 the XRD indicates there is still a significant range of crystalline mineral components, and the reactivity was less affected than demineralisation of the hydrochar.

3.2.3. Characterisation of surface chemistry and CO_2 chemisorption

The XPS analyses of the samples shown in Table 5 were used to give an insight into the chemical groups present on the surface, and to help explain the differences in reactivity with a view to optimising CO_2 reactivity. Considering the relationship between the ash content and the reactivity of the hydrochar, as demonstrated by the demineralisation, the surface functionality of the hydrochar is expected to play a dominant role on the gas–solid gasification reactivity.

In comparison to the other tests used, XPS is a powerful surface analysis technique which gives a more detailed description of the area dominated by gas–solid interactions, i.e. at the surface. XRD and SEM-EDS analyses only identify the crystalline phases and ICP is a bulk analysis technique.

The hydrochar sample (HC) had the highest surface concentrations of calcium and iron, both of which are known to catalyse gasification reactions. BC3 & BC4 also both had high concentrations of calcium while BC1 & BC2 had potassium on the sample surface, which has also been identified as an important gasification catalyst.

An often-overlooked parameter to gasification reactivity is the form of carbon present on the surface. The XPS can be used to determine the

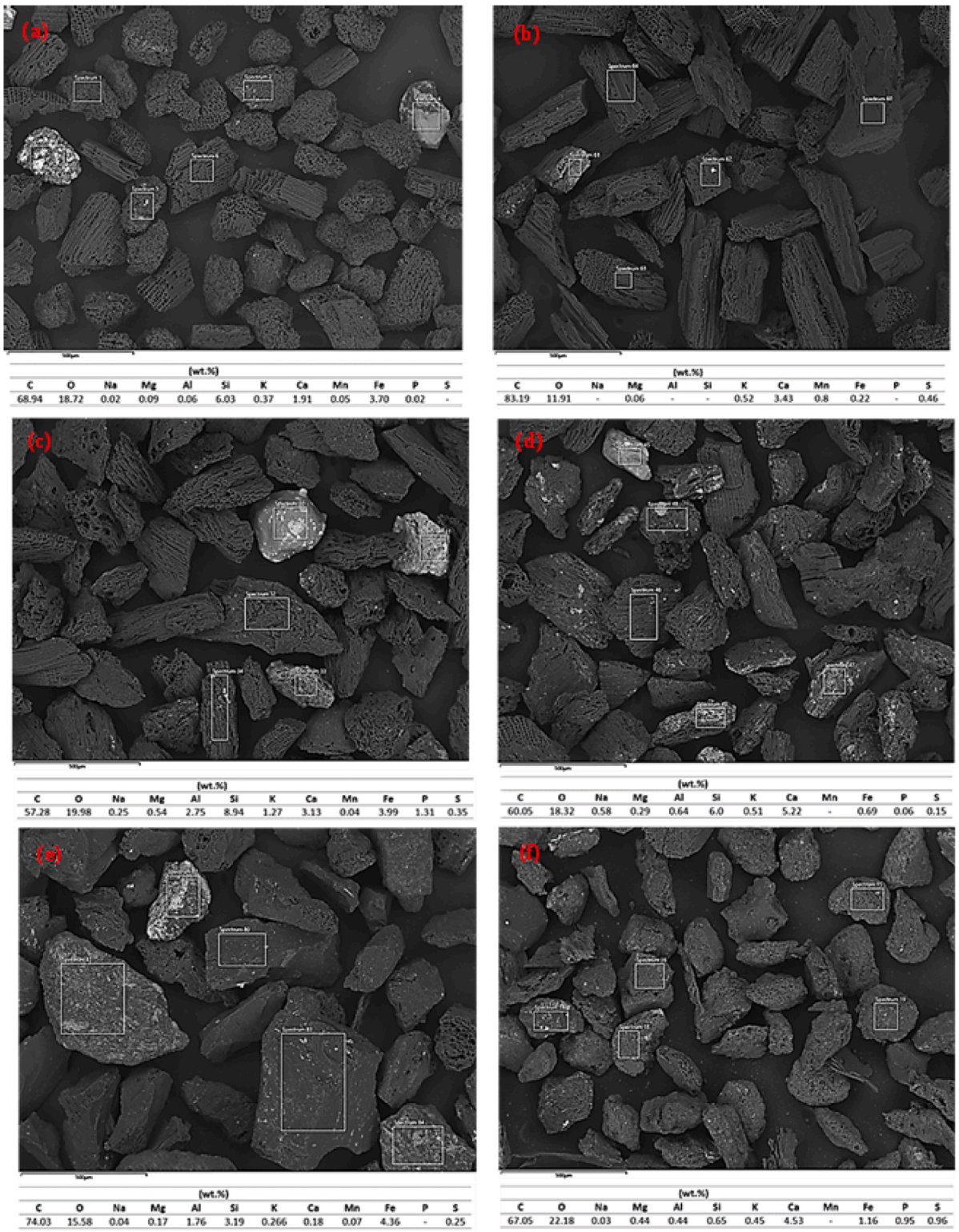

Fig. 8. Backscattered EDS analysis of semi-quantitative and elements distribution on char surfaces taken in back scattered mode at 500X magnification: (a)BC1, (b) BC2, (C) BC3, (d) BC4, (e) CC and (f) HC.

sp^2/sp^3 carbon hybridisation bonding using the X-ray excited carbon auger (C_{KLL}) spectra. This was first carried out by Lascovich and Scalione and quoted as the D-parameter derived from the differential of the carbon auger signal [39] (Table 6). The proposal involves a linear approximation for the parameter ranging from diamond-like (100 % in the sp^3 configuration) where D = 14 eV; to graphitic-like carbon at 23 eV where the carbons are 100 % in their sp^2 configuration.

Other researchers have shown associations between the more structurally ordered graphitic sp^2 type bonding and lower reactivity as associated with aromatic ring structures compared to the less structurally ordered sp^3 type bonding. This is consistent for the hydrochar sample in Table 6 which has a low sp^2 content and its higher gasification reactivity, but less obvious with the other biochars which vary from 0 to 94 % sp^2 bonding, but exhibit less variability in the reactivity compared

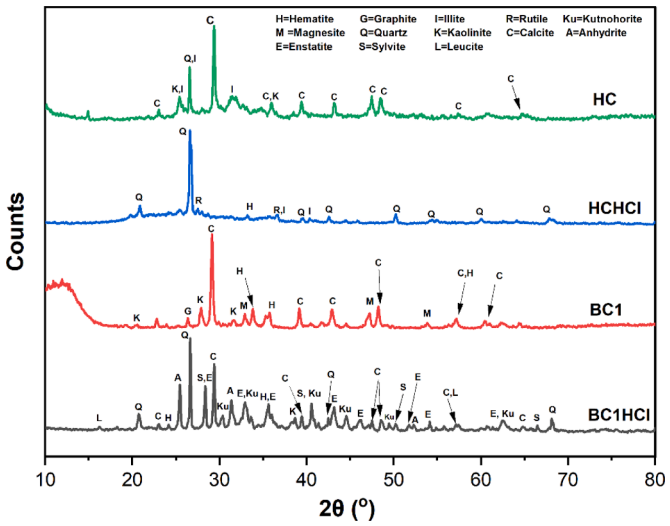

Fig. 9. XRD patterns of BC1, HC and their demineralised chars BC1HCl HCHCl.

Table 4
Semi-quantification of the crystalline phases of the biochar and hydrochar samples and their demineralised chars obtained from XRD analysis of the ash (absolute wt.% of dried sample).

Mineral	BC1	BC1HCl	HC	HCHCl
Calcite	2.9	0.34	11.0	0.0
Graphite	0.32	0.0	0.0	0.0
Hematite	0.70	0.18	0.0	0.23
Illite	0.0	0.0	3.09	0.22
Kaolinite	0.28	0.19	3.8	0.0
Magnesite	0.47	0.0	0.0	0.0
Quartz	0.0	0.47	2.9	3.2
Sylvite	0.0	0.38	0.0	0.0
Leucite	0.0	0.14	0.0	0.0
Rutile	0.0	0.0	0.0	0.11
Enstatite	0.0	0.64	0.0	0.0
Anhydrite	0.0	0.32	0.0	0.0
Kutnohorite	0.0	0.10	0.0	0.0

to each other. The D-parameters indicate that hybridised bonding of BC1 and HC remains predominantly sp^3 after acid washing showing no evidence of a significant change in the type of carbon.

Analysis of the Carbon, C(1s) and Oxygen, O(1s) core-levels (Fig. 10), reveal significant differences in the surface functionalities of the chars. Where significant oxygen functionality exists (HC, BC1 and CC), the materials exhibit some carbonyl containing functionalities, as evidenced by peaks above *ca.* 287 eV and pi-pi* signal in the corresponding O(1s) peak (typically this is observed above *ca.* 534 eV).

The spectra for HC and BC1 contain ether and alcohol (C-O-C/C-OH) moieties (*ca.* 286 eV and 532 eV for C(1s) and O(1s) respectively). A deeper understanding of the O(1s) peaks is complicated by the presence of other inorganic elements, such as sulphur and calcium, all of which are in their oxidic and/or hydroxide forms and have binding energies similar to those bound to carbon.

The wider C(1s) peak asymmetry indicates more types of functional surface bonding which could play a role in facilitating chemisorption of CO_2 onto the surface. This is greatest for the most reactive hydrochar and the BC1; both show peaks with binding energies around 287.5 eV corresponding to carbonyl groups (C=O) and 288.5 eV corresponding to carboxyl (typically acid groups) and ester groups (from the formation of acid and alcohol reactions). The different type of carbon–oxygen bonding sets up dipole moments with asymmetric electron distribution that could play an important role in facilitating the CO_2 combination on the surface.

Several studies have been carried out to establish a connection between the chemical adsorption of CO_2 molecules on the char surface and the reactivity of char gasification [30,40,41]. Continuing from the XPS surface analysis, the CO_2 chemisorption capacities of char samples are shown in Fig. 11. The chemisorption is split into two parameters based on the characterisation of the chemisorption as weak and strong, denoted in the figure as C_{wea} and C_{str} and has been related to the organic and inorganic components of the char [29,40].

The hydrothermal char (HC) had the highest C_{str} value of 13.60 mg of CO_2/g of char which corresponds to its high reactivity. This amount of CO_2 chemisorbed on HC was expected as one of the advantages of such char is its adsorption capability [42–44], which is greater than biochars [45–47]. The C_{str} values of woody biochars, BC1 and BC2, were 4.37 and 3.32 mg of CO_2/g of char respectively while the sewage sludge chars, BC3 and B4, had comparable C_{str} values to the coal but lower C_{wea}.

The C_{wea} has been linked to reversible interactions with organic active sites and other researchers have questioned if the weak interaction is a predictor of char gasification reactivity [40,48]. For this study coal char, CC, has the highest capacity of C_{wea} of 7.73 mg of CO_2/g but a much smaller C_{str} and a correspondingly lower reactivity.

After demineralisation, both BC1HCl and HCHCl show a significant reduction in strong chemisorption capacities replaced by a corresponding increase in weak chemisorption. As shown in Fig. 11, the amount of irreversible CO_2 strong chemisorption (C_{str}) of BC1 and HC decreased by 68 % and 85 % respectively. The demineralisation of the chars appears to reduce the strength of CO_2 chemisorption with a corresponding reduction in reactivity, suggesting that the ash minerals play

Table 6
XPS Carbon auger (CKLL) D-parameter and sp hybridised bonding.

Sample	D-Parameter	%sp^2	%sp^3
BC1	14.0	0.00	100.0
BC2	18.0	44.0	56.0
BC3	22.5	94.0	6.0
BC4	22.0	89.0	11.0
CC	18.0	44.00	56.0
HC	15.5	12.0	88.0
BC1HCl	15	10	90
HCHCl	14.5	3	97

Table 5
Surface atomic concentrations for each carbon sample.

Sample	Elemental at%										
	Al 2p	C 1s	Ca 2p	Cl2p	Fe 2p	Co 2p	N 1s	Na 1s	O 1s	S 2p	K 2p
BC1	0	75.47	0.21	0	0	0	0.35	0.14	23.24	0	0.59
BC2	0	91.22	0.43	0.07	0	0	0.42	0	7.55	0	0.31
BC3	0.37	90.59	0.86	0.18	0.28	0	0.42	0.19	6.76	0.35	0
BC4	0.13	91.9	0.93	0.54	0	0.04	0.57	0.22	5.51	0.16	0
CC	1.4	83.35	0.2	0	0.12	0.08	1.66	0	12.84	0.35	0
HC	1.01	67.64	1.85	0	0.5	0	3.45	0	25.11	0.44	0
BC1HCl	0	75.25	0	0	0	0	3.69	0	22.26	0.41	0
HCHCl	0	73	0	0	0	0	4.13	0	21.14	0.32	0

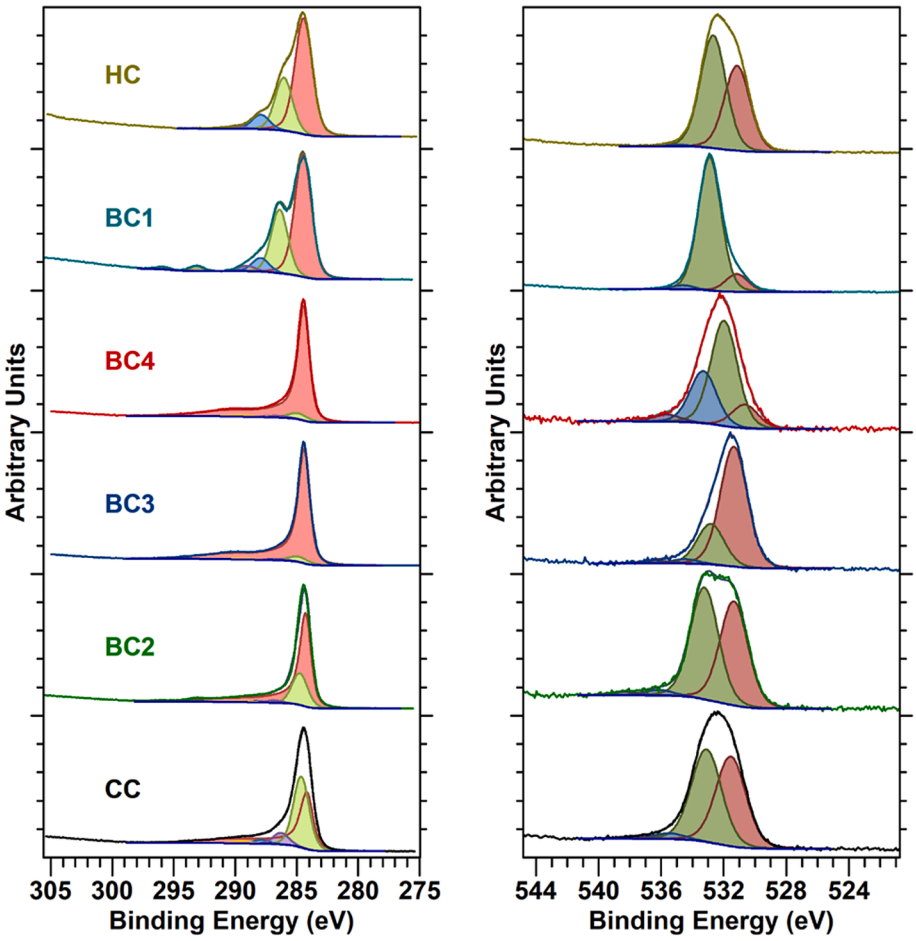

Fig. 10. C(1 s) and O(1 s) core-level spectra for each material studied.

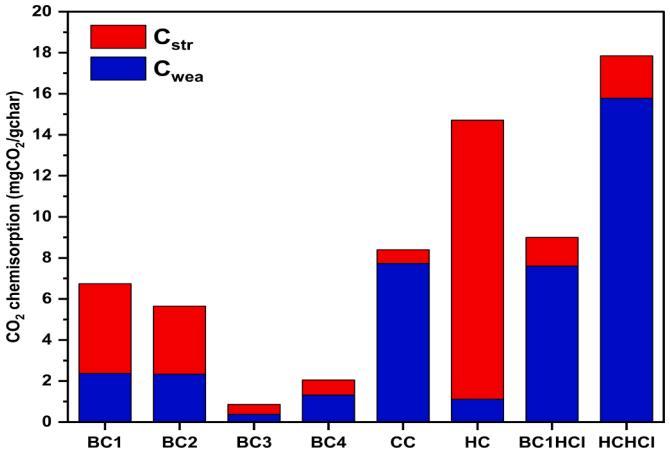

Fig. 11. Strong and weak CO2 chemisorption (Cstr, Cwea) for char samples.

a direct role in the mechanism of CO_2 surface reactions.

A closer look at the relationship between the reactivity of chars and C_{str} is shown in Fig. 12. The high values of R^2 of 0.924, 0.919, and 0.890, indicate a strong linear correlation between C_{str} and chars reactivity in the temperature range studied, and a similar positive correlation was recently reported by other investigations [49].

3.3. Kinetic analyses

The following analysis of the reaction kinetics has been carried out to better understand the dominant mechanisms of the gasification reactions and determine the kinetic parameters for the relation with the previous findings using linearised forms of equations (6)–(8), which were plotted against conversion time at 900 °C to 1000 °C as shown in Fig.S3 (supplementary data).

The reaction rate constants, k_{VM}, k_{GM} and k_{RPM} were determined by obtaining the slope of each plot derived from the resultant linear relationship, which corresponded to the models of VM, GM, and RPM, respectively. The optimum fitting was used to estimate the structural parameter, ψ values in the RPM case. These values remained constant across varying temperatures due to their association with the initial pore structure of the chars [28]. The reaction rate constant values were significantly increased when the reaction temperature increased from 900 °C to 1000 °C for all the kinetic methods as shown in Fig 13.. These results indicate that the gasification temperature is the most important factor controlling the reaction rate and is with agreement with results found in the literature [50].

The calculated reaction constants from VM, GM and RPM were used to plot Arrhenius curves by plotting (lnk) vs. ($1/T$) to determine the kinetic parameters, activation energy E_a and the pre-exponential factor A_0. According to Fig.S4 (supplementary data), a good linear relationship is observed between (lnk) and ($1/T$) for the chars at the gasification temperatures which indicates that the process is governed by the chemical reaction [28]. The fitting curves at different temperatures were obtained by fitting the experimental results of CO_2 gasification to the kinetic models, as shown in Fig.S5 (supplementary data). The RPM

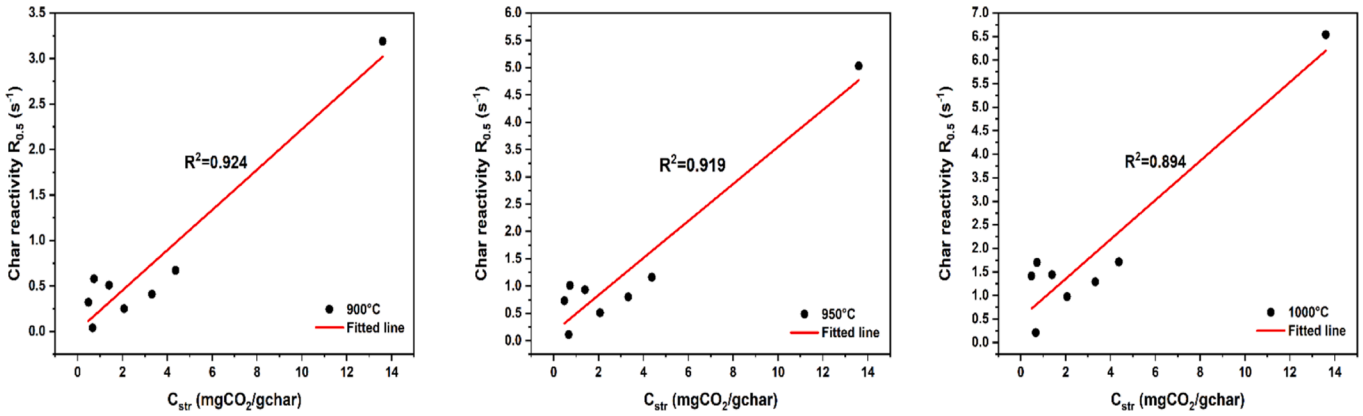

Fig. 12. Correlations of the strong CO2 chemisorption (Cstr) with gasification reactivities at 900 °C, 950 °C, and 1000 °C.

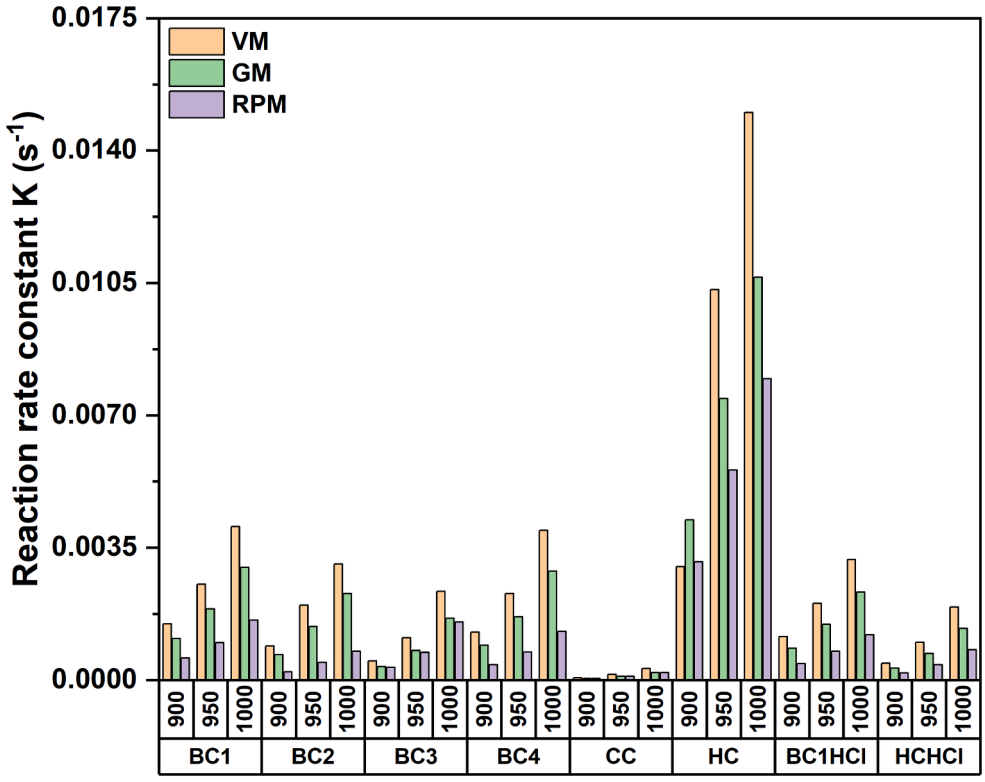

Fig. 13. Reaction rate constants obtained from VM, GM and RPM.

Table 7
Kinetic parameters obtained by VM, GM and RPM models for the char samples.

Sample	VM		GM		RPM		
	E(kJ/mol)	A_0(s^{-1})	*E*(kJ/mol)	A_0(s^{-1})	*E*(kJ/mol)	A_0(s^{-1})	ψ
BC1	125.2	559.2	123.7	354.9	124.9	210.7	7.7
BC2	153.6	6510.7	153.2	4575.2	155.6	1902.5	23.6
BC3	179.9	55547.8	180.0	39183.1	180.3	37949.1	1.3
BC4	142.4	2760.3	142.3	1986.2	143.9	1036.4	11.7
CC	193.6	26903.2	188.7	11385.6	190.3	13550.8	1.0
HC	114.0	733.4	114.9	568.2	116.2	479.4	2.9
BC1HCl	126.6	506.7	126.1	351.7	126.5	187.8	8.1
HCHCl	184.1	70615.2	183.0	44891.3	183.7	27694.8	5.7

model provides the most optimal fit for gasification data of the biomass chars and hydrochar under investigation at all temperatures studied. This finding is consistent with the existing literature [22,28,51–53].

The effect of demineralisation on the hydrochar (HCHCl at 900 °C and 950 °C) was a change from the best fit as the random pore model to the grain model instead, whilst maintaining similar kinetic parameters

Table 8
Activation energy values of chars in literature for isothermal CO_2 gasification.

Material	Temperature (°C)	Kinetic model	E(kJ/mol)	Reference
Herbaceous & wooden residues	850–1000	RPM	129.8–180.3	[28]
Barapukurian bituminous coal	800–1100	VM, GM and RPM	171.2–173.7	[24]
Bituminous coal	1050–1150	GM	125–207.6	[54]
Food waste	850–950	VM, GM and RPM	155–164.3	[55]
Pinus densiflora	850–1050	VM, GM and RPM	134–172	[56]

Table 9
Deviation between the predicted values by the kinetic models (VM, GM and RPM) a and the experimental data.

Sample	*DEV X (%)*		
	VM	GM	RPM
BC1	15.03	10.10	3.77
BC2	16.17	11.15	3.49
BC3	4.02	3.10	2.99
BC4	15.02	9.79	2.41
CC	2.24	5.69	4.60
HC	12.72	7.24	4.76
BC1HCl	13.71	8.44	2.06
HCHCl	9.02	3.28	3.45

suggesting a change in the reaction mechanism of HC with the loss of catalytic ash components. The kinetic parameters of HC were measurably changed after demineralisation with significant increases in activation energies for HC from 116.2 to 183.0 kJ/mol whereas BC1 was much less affected ranging from 124.9 to 126.5 kJ/mol as shown in Table 7. In this study, the activation energy values obtained from the kinetic models ranged between 114 to 193.6 kJ/mol. These values fall within the activation energy values, as reported in the literature and shown in Table 8. Although, the activation energy of HC is slightly lower, this may be attributed to the hydrothermal treatment applied to this sample. The range of techniques used to analyse and compare the samples used in this study, including demineralisation, illustrates the potential contribution of other reaction mechanisms on the activation energy. In particular, the advanced surface analysis using XPS identified increased chemical surface functionality for the HC and BC1 samples. This was indicated by wide asymmetric carbon peaks, and the predominately sp^3 allotropic form of carbon and correspondingly lower activation energies.

In comparison, experimental conversion profiles of CC were fitted by the VM indicating that coal char has a completely different mechanism compared to biomass chars. Table 8 presents a summary of the result of the deviation test between the experimental data and the kinetic models based on Eq.10. The results show that relative errors corresponding to the RPM are the lowest of all models except for CC and demineralised hydrochar (HCHCl) as shown in Table 9.

4. Conclusions

In this work, char samples were reacted with CO_2 at high temperatures to examine their reactivities during gasification using TGA and detailed surface analysis techniques. A demineralisation treatment was performed to investigate the ash composition influence on chars' reactivity. Moreover, CO_2 chemisorption method was used to evaluate char surface adsorption and desorption capacities. The following conclusions were therefore drawn:

1. Biochars have much better CO_2 gasification reactivity compared to coal chars and are strong candidates for consideration in a carbon utilisation reaction to produce carbon monoxide for the synthesis of platform chemicals. The shorter reactivity time at lower temperatures will result in lower energy requirements to carry out the carbon utilisation reaction compared to other materials.
2. XPS gave a valuable insight into the type of functional chemical groups associated with the highest reactivity chars. The hydrochar and the BC1 surfaces both showed a wide range of functional chemical groups such as carbonyl, ester and carboxyl groups. It was less clear however what role the sp^2/sp^3 bonding played for all the chars; although the highest reactivity chars did correspond with lower sp^2 bonding in agreement with other literature findings.
3. The reduction in the ash content by demineralisation of the chars reduces the strong CO_2 chemisorption and also relates to the rate of reaction. The results suggest minerals play a role in the mechanism by which CO_2 combines with carbon on the surface of the chars but there is some variation on its importance depending on the sample.
4. According to physicochemical properties of chars there is more than one parameter controlling CO_2 gasification reactivity of chars at high temperature. While the pore structure of chars is indeed a significant characteristic, it appears that porosity alone does not exert the primary influence on gasification reactivity. This conclusion is supported by the findings of analytical techniques, which indicate that the types of inorganic elements present and their distribution on the surface may be more closely associated with the observed variations in reactivity.
5. The impact of demineralisation treatment on hydrochar was stronger than biochar, suggesting that the dominant factor of HC reactivity is the presence of the minerals and their catalytic affect.
6. The CO_2 chemisorption procedure can be used as an evaluation tool to predict different chars reactivities, i.e. gasification reactivity is well correlated with CO_2 strong chemisorption C_{str}.
7. Three kinetic models, namely, VM, GM and RPM were used to describe CO_2 gasification of the different samples by fitting experimental data with models and results show that:

a. The reaction rate constant values were significantly increased when the reaction temperature increased from 900 °C to 1000 °C for all the kinetic models.
b. The RPM model provides the most optimal fit for gasification data of the biomass chars and hydrochar under investigation at all temperatures. CC was fitted by the VM indicating that coal char has a completely different mechanism compared to biomass chars.
c. The RPM model was reduced to the GM model for the demineralised hydrochar at 900 °C and 950 °C, which suggests that the reaction mechanism of HC is different after demineralisation.

CRediT authorship contribution statement

Ahmed Mohammed Alsawadi: Writing – review & editing, Writing – original draft, Visualization, Validation, Software, Methodology, Investigation, Formal analysis, Conceptualization. **Richard Marsh:** Writing – review & editing, Supervision, Resources, Project administration. **Julian M. Steer:** Writing – review & editing, Supervision, Resources, Project administration. **David Morgan:** Investigation, Formal analysis.

Declaration of competing interest

The authors declare that they have no known competing financial interests or personal relationships that could have appeared to influence the work reported in this paper.

Appendix A. Supplementary material

Supplementary data to this article can be found online at https://doi.org/10.1016/j.fuel.2024.133448.

Data availability

Data will be made available on request.

References

[1] Gabrielli P, Gazzani M, Mazzotti M. The role of carbon capture and utilization, carbon capture and storage, and biomass to enable a net-Zero-CO_2 emissions chemical industry. Ind Eng Chem Res 2020;59:7033–45. https://doi.org/10.1021/acs.iecr.9b06579.

[2] Gulzar A, Gulzar A, Ansari MB, He F, Gai S, Yang P. Carbon dioxide utilization: A paradigm shift with CO_2 economy. Chem Eng J Adv 2020;3:100013. https://doi.org/10.1016/J.CEJA.2020.100013.

[3] International Energy Agency (IEA) 2019. Putting CO2 to Use. Paris 2019. https://www.iea.org/reports/putting-co2-to-use.

[4] Kim C, Yoo CJ, Oh HS, Min BK, Lee U. Review of carbon dioxide utilization technologies and their potential for industrial application. J CO_2 Util 2022;65:102239. https://doi.org/10.1016/J.JCOU.2022.102239.

[5] Saravanan A, Senthil kumar P, DVN Vo, Jeevanantham S, Bhuvaneswari V, Anantha Narayanan V, et al. A comprehensive review on different approaches for CO_2 utilization and conversion pathways. Chem Eng Sci 2021;236:116515. https://doi.org/10.1016/J.CES.2021.116515.

[6] Zhang Z, Pan SY, Li H, Cai J, Olabi AG, Anthony EJ, et al. Recent advances in carbon dioxide utilization. Renew Sustain Energy Rev 2020;125:109799. https://doi.org/10.1016/j.rser.2020.109799.

[7] Okoye-Chine CG, Otun K, Shiba N, Rashama C, Ugwu SN, Onyeaka H, et al. Conversion of carbon dioxide into fuels—a review. J CO_2 Util 2022;62:102099. https://doi.org/10.1016/J.JCOU.2022.102099.

[8] Nimmas T, Wongsakulphasatch S, Chanthanumataporn M, Vacharanukrauh T, Assabumrungrat S. Thermochemical transformation of CO_2 into high-value products. Curr Opin Green Sustain Chem 2024;47:100911. https://doi.org/10.1016/J.COGSC.2024.100911.

[9] Nagireddi S, Agarwal JR, Vedapuri D. carbon dioxide capture, utilization, and sequestration: current status, challenges, and future prospects for global decarbonization. ACS Eng Au 2023;4:22–48. https://doi.org/10.1021/ACSENGINEERINGAU.3C00049.

[10] Turakulov Z, Kamolov A, Norkobilov A, Variny M, Díaz-Sainz G, Gómez-Coma L, et al. Assessing various CO_2 utilization technologies: a brief comparative review. J Chem Technol Biotechnol 2024;99:1291–307. https://doi.org/10.1002/JCTB.7606.

[11] Hasan MMF, Rossi LM, Debecker DP, Leonard KC, Li Z, Makhubela BCE, et al. Can CO_2 and renewable carbon be primary resources for sustainable fuels and chemicals? ACS Sustain Chem Eng 2021;9:12427–30. https://doi.org/10.1021/ACSSUSCHEMENG.1C06008.

[12] Huang J, Zhang H, Tan Q, Li L, Xu R, Xu Z, et al. Enhanced conversion of CO_2 into O_2-free fuel gas via the Boudouard reaction with biochar in an atmospheric plasmatron. J CO_2 Util 2021;45:101429. https://doi.org/10.1016/J.JCOU.2020.101429.

[13] Wang T. An overview of IGCC systems. In: Wang T, Stiegel GBT-IGCC (IGCC) T, editors. Integr. Gasif. Comb. Cycle Technol., Woodhead Publishing; 2017, p. 1–80. doi: 10.1016/B978-0-08-100167-7.00001-9.

[14] Steer JM, Marsh R, Morgan D, Greenslade M. The effects of particle grinding on the burnout and surface chemistry of coals in a drop tube furnace. Fuel 2015;160:413–23. https://doi.org/10.1016/j.fuel.2015.07.094.

[15] Snape CE, Meredith W, McKechnie J, West H, Rodgers S, Stephens L, et al. BEIS GGR Innovation Phase 1 Project Bio-waste to Biochar (B to B) via Hydrothermal Carbonisation and Post-Carbonisation Final Report n.d. https://assets.publishing.service.gov.uk/government/uploads/system/uploads/attachment_data/file/1091764/university-nottingham-biowaste-to-biochar.pdf (accessed October 15, 2023).

[16] Kolosionis A, Kastanaki E, Veksha A, Wang H, He C, Lisak G, et al. The effects of washing techniques on thermal combustion properties of sewage sludge chars. Int J Environ Res 2021;15:285–97. https://doi.org/10.1007/S41742-021-00312-6.

[17] Fairley N, Fernandez V, Richard-Plouet M, Guillot-Deudon C, Walton J, Smith E, et al. Systematic and collaborative approach to problem solving using X-ray photoelectron spectroscopy. Appl Surf Sci Adv 2021;5:100112. https://doi.org/10.1016/J.APSADV.2021.100112.

[18] Takarada T, Tamai Y, Tomita A. Reactivities of 34 coals under steam gasification. Fuel 1985;64:1438–42. https://doi.org/10.1016/0016-2361(85)90347-3.

[19] Steer J, Greenslade M, Marsh R. A comparison of laboratory coal testing with the blast furnace process and coal injection. Metals (Basel) 2021;11. https://doi.org/10.3390/met11091476.

[20] Roncancio R, Gore JP. CO_2 char gasification: a systematic review from 2014 to 2020. Energy Convers Manag X 2021:10. https://doi.org/10.1016/J.ECMX.2020.100060.

[21] Ishida M, Wen CY. Comparison of zone-reaction model and unreacted-core shrinking model in solid-gas reactions-I isothermal analysis. Chem Eng Sci 1971;26:1031–41. https://doi.org/10.1016/0009-2509(71)80017-9.

[22] Htet TT, Yan Z, Spooner S, Degirmenci V, Meijer K, Li Z. Gasification and physical-chemical characteristics of carbonaceous materials in relation to HIsarna ironmaking process. Fuel 2021;289:119890. https://doi.org/10.1016/J.FUEL.2020.119890.

[23] Lopez G, Alvarez J, Amutio M, Arregi A, Bilbao J, Olazar M. Assessment of steam gasification kinetics of the char from lignocellulosic biomass in a conical spouted bed reactor. Energy 2016;107:493–501. https://doi.org/10.1016/j.energy.2016.04.040.

[24] Shahabuddin M, Kibria MA, Bhattacharya S. Gasification kinetics of Barapukurian coal char using carbon dioxide and steam reactants. Chem Pap 2022;76:4459–70. https://doi.org/10.1007/S11696-022-02186-0/FIGURES/14.

[25] Szekely J, Evans JW. A structural model for gas-solid reactions with a moving boundary. Chem Eng Sci 1970;25:1091–107. https://doi.org/10.1016/0009-2509(70)85053-9.

[26] Bhatia SK, Perlmutter DD. A rondom pore model for fluid-solid reactions: i. isothermal, kinetic control. AIChE J 1980;26:379–86. https://doi.org/10.1007/978-3-319-89554-3.

[27] Bhatia SK, Perlmutter DD. A random pore model for fluid-solid reactions : II diffusion and transport effects. AIChE J 1981;27:247–54.

[28] Wang G, Zhang J, Shao J, Liu Z, Wang H, Li X, et al. Experimental and modeling studies on CO_2 gasification of biomass chars. Energy 2016;114:143–54. https://doi.org/10.1016/J.ENERGY.2016.08.002.

[29] Xu K, Hu S, Su S, Xu C, Sun L, Shuai C, et al. Study on char surface active sites and their relationship to gasification reactivity. Energy Fuel 2012;27:118–25. https://doi.org/10.1021/ef301455x.

[30] Jing X, Wang Z, Zhang Q, Yu Z, Li C, Huang J, et al. Evaluation of CO_2 gasification reactivity of different coal rank chars by physicochemical properties. Energy Fuel 2013;27:7287–93. https://doi.org/10.1021/EF401639V.

[31] Lahijani P, Mohammadi M, Mohamed AR. Catalytic CO_2 gasification of rubber seed shell-derived hydrochar: reactivity and kinetic studies. Environ Sci Pollut Res 2019;26:11767–80. https://doi.org/10.1007/s11356-019-04613-4.

[32] Thommes M, Kaneko K, Neimark AV, Olivier JP, Rodriguez-reinoso F, Rouquerol J, et al. Physisorption of gases, with special reference to the evaluation of surface area and pore size distribution (IUPAC Technical Report). J Pure Appl Chem 2015;87:1051–69. https://doi.org/10.1515/pac-2014-1117.

[33] Schmidt HP, Bucheli T, Kammann C, Glaser B, Abiven S, Leifeld J, et al. European Biochar Certificate - Guidelines for a Sustainable Production of Biochar. Eur Biochar Found 2023;10.

[34] Al-Ghouti MA, Da'ana DA. Guidelines for the use and interpretation of adsorption isotherm models: A review. J Hazard Mater 2020;393:122383. https://doi.org/10.1016/j.jhazmat.2020.122383.

[35] Müller FJ, Fuchs J, Fanjul Cuesta M, Oblanca Gutiérrez A, Pratschner S, Müller S, et al. CO_2 conversion to CO by fluidized bed biomass gasification: Analysis of operational parameters. J CO_2 Util 2024;81:102706. https://doi.org/10.1016/J.JCOU.2024.102706.

[36] Wang Q, Wang E, Li K, Husnain N, Li D. Synergistic effects and kinetics analysis of biochar with semi-coke during CO_2 co-gasification. Energy 2020;191:116528. https://doi.org/10.1016/J.ENERGY.2019.116528.

[37] Trueman C. Geochemistry | inorganic. Encycl Anal Sci Second Ed 2005:171–81. https://doi.org/10.1016/B0-12-369397-7/00240-5.

[38] Wajima T. Effects of step-wise acid leaching with HCl on synthesis of zeolitic materials from paper sludge ash. Miner 2020;10:402. https://doi.org/10.3390/MIN10050402.

[39] Morgan DJ. Comments on the XPS Analysis of Carbon Materials. C 2021, Vol 7, Page 51 2021;7:51. doi: 10.3390/C7030051.

[40] Molina A, Montoya A, Mondragón F. CO_2 strong chemisorption as an estimate of coal char gasification reactivity. Fuel 1999;78:971–7. https://doi.org/10.1016/S0016-2361(98)00220-8.

[41] Jiao WW, Wang Z, Jiao WW, Li L, Zuo Z, Li G, et al. Influencing factors and reaction mechanism for catalytic CO_2 gasification of sawdust char using K-modified transition metal composite catalysts: experimental and DFT studies. Energy Convers Manag 2020;208:112522. https://doi.org/10.1016/j.enconman.2020.112522.

[42] Zhang F, Wu Q. Functional materials development from kitchen waste. Procedia Environ Sci 2012;16:70–4. https://doi.org/10.1016/j.proenv.2012.10.010.

[43] Luo Y, Lan Y, Liu X, Xue M, Zhang L, Yin Z, et al. Hydrochar effectively removes aqueous Cr(VI) through synergistic adsorption and photoreduction. Sep Purif Technol 2023;317:123926. https://doi.org/10.1016/j.seppur.2023.123926.

[44] Qiu M, Liu L, Ling Q, Cai Y, Yu S, Wang S, et al. Biochar for the removal of contaminants from soil and water: a review. Biochar 2022;4:1–25. https://doi.org/10.1007/S42773-022-00146-1/FIGURES/7.

[45] Goel C, Mohan S, Dinesha P. CO_2 capture by adsorption on biomass-derived activated char: a review. Sci Total Environ 2021;798:149296. https://doi.org/10.1016/j.scitotenv.2021.149296.

[46] Masoumi S, Borugadda VB, Nanda S, Dalai AK. Hydrochar: A review on its production technologies and applications. Catalysts 2021;11:939. https://doi.org/10.3390/catal11080939.

[47] Qambrani NA, Rahman MM, Won S, Shim S, Ra C. Biochar properties and eco-friendly applications for climate change mitigation, waste management, and wastewater treatment: A review. Renew Sustain Energy Rev 2017;79:255–73. https://doi.org/10.1016/J.RSER.2017.05.057.

[48] Zhang Y, Hara S, Kajitani S, Ashizawa M. Modeling of catalytic gasification kinetics of coal char and carbon. Fuel 2010;89:152–7. https://doi.org/10.1016/J.FUEL.2009.06.004.

[49] Guo S, Jiang Y, Liu T, Zhao J, Huang J, Fang Y. Investigations on interactions between sodium species and coal char by thermogravimetric analysis. Fuel 2018;214:561–8. https://doi.org/10.1016/j.fuel.2017.11.069.

[50] Tian H, Hu Q, Wang J, Chen D, Yang Y, Bridgwater AV. Kinetic study on the CO_2 gasification of biochar derived from Miscanthus at different processing conditions. Energy 2021;217:119341. https://doi.org/10.1016/j.energy.2020.119341.

[51] Song Q, Wang X, Gu C, Li H, Huo J. Study on CO_2 gasification kinetics of biomass char based on pore structure analysis: Theoretical modelling of structural

parameter ψ in random pore model. Int J Energy Res 2021;45:4429–42. https://doi.org/10.1002/ER.6113.
[52] Wang G, Ren S, Zhang J, Ning X, Liang W, Zhang N, et al. Influence mechanism of alkali metals on CO_2 gasification properties of metallurgical coke. Chem Eng J 2020;387:124093. https://doi.org/10.1016/J.CEJ.2020.124093.
[53] Liu Z, Wang G, Zhang J, Lee JY, Wang H, Sun M, et al. Study on CO_2 Gasification reactivity and structure characteristics of carbonaceous materials from the corex furnace. Energy Fuel 2018;32:6155–66. https://doi.org/10.1021/acs.energyfuels.8b00072.
[54] Kim YT, Seo DK, Hwang J. Study of the effect of coal type and particle size on char-CO_2 gasification via gas analysis. Energy Fuel 2011;25:5044–54. https://doi.org/10.1021/ef200745x.
[55] Izaharuddin AN, Paul MC, Yoshikawa K, Theppitak S, Dai X. Comprehensive kinetic modeling study of CO_2 gasification of char derived from food waste. Energy Fuel 2020;34:1883–95. https://doi.org/10.1021/acs.energyfuels.9b03937.
[56] Seo DK, Lee SK, Kang MW, Hwang J, Yu TU. Gasification reactivity of biomass chars with CO_2. Biomass Bioenergy 2010;34:1946–53. https://doi.org/10.1016/J.BIOMBIOE.2010.08.008.